How to cite: *Angew. Chem. Int. Ed.* **2024**, *63*, e202314112
doi.org/10.1002/anie.202314112

Photochemistry

Wavelength Selective Photocontrol of Hybrid Azobenzene-Spiropyran Photoswitches with Overlapping Chromophores

Torben Saßmannshausen[+], Anne Kunz[+], Nils Oberhof[+], Friederike Schneider, Chavdar Slavov, Andreas Dreuw, Josef Wachtveitl,* and Hermann A. Wegner**

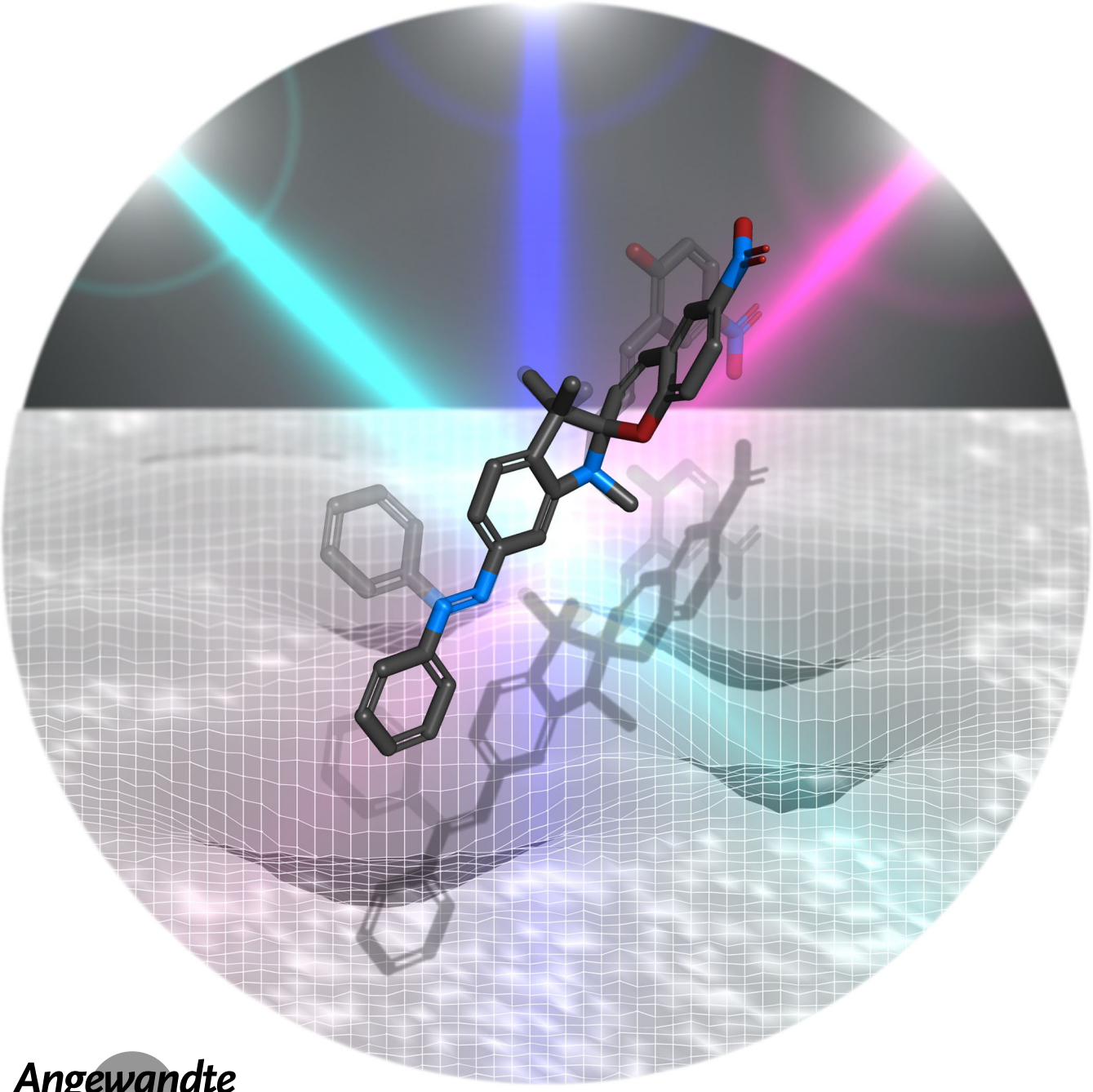

Abstract: Compounds with multiple photoswitching units are appealing for complex photochemical control of molecular materials and nanostructures. Herein, we synthesized novel *meta*- and *para*- connected (related to the nitrogen of the indoline) azobenzene-spiropyran dyads, in which the central benzene unit is shared by both switches. We investigated their photochemistry using static and time-resolved transient absorption spectroscopy as well as quantum chemical calculations. In the *meta*-compound, the individual components are photochemically decoupled due to the *meta*-pattern. In the *para*-compound the spiro-connectivity leads to a bifunctional photoswitchable system with a red-shifted absorption. The azobenzene and the spiropyran can thus be addressed and switched independently by light of appropriate wavelength. Through the different connectivity patterns two different orthogonally photoswitchable systems have been obtained which are promising candidates for complex applications of light control.

Introduction

Building on the individual properties of monomeric photoswitches, multiphotochromic compounds consisting of two or more photoswitches offer new attractive possibilities for wavelength-selective applications in nanotechnology,[1–3] renewable energy utilization,[4,5] data storage and modification.[6] Meanwhile, the development of such molecular composite systems with new emergent functionalities poses challenges to synthesis, spectroscopy and theory. In general, it is not clear *a priori* what the ideal way is to covalently link photoswitches to achieve the desired wavelength-dependent functionality. In fact, the isomerization dynamics of the individual subunits of linked azobenzenes (ABs) and thus their multifunctional switching behavior strongly depends on their specific connectivity pattern.[7–10] While *meta*-bis-AB shows a similar absorption spectrum, dynamics and only slightly reduced quantum efficiency compared to the monomeric AB, *para*-bis-AB has a strongly red-shifted absorption band, strongly altered dynamics and a lower quantum efficiency. From these findings the so-called "*meta*-rule" was derived, according to which the individual photoswitches are decoupled in the *meta* connectivity pattern.[11,12] However, due to symmetry and resulting spectral overlap, selective excitation of the individual AB units has not yet been achieved.[9]

In some works, this addressability issue has been targeted by orthogonally accessible hybrid dimers, like for instance the connection of an AB with a Stenhouse adduct or spiropyran (SP) via a linker (Figure 1).[13–16] Additionally, Wilson et al. achieved orthogonal switching of a SP and a diarylethene within a metal–organic framework.[17] In such hybrid systems the constituent moieties possess sufficiently large spectral separation allowing for individual excitation. At the same time, hybrid systems often possess expanded spectral coverage. Ideally, they show enriched physicochemical properties, such as higher information or energy density. However, these properties usually come at the expense of more complex photophysics and photochemistry, since combining two photoswitches often opens new photochemical pathways, like energy, electron or proton transfer not present in the individual monomers. Along these lines, we designed two new hybrid AB-SP dyads in which an AB moiety is directly connected to the indoline moiety of SP, either at the *meta*- or *para*-position relative to the SP-nitrogen (Figure 1). Thus, the two moieties of the hybrid switch share the indoline ring resulting in a highly compact and atom-efficient structure. One major issue of such covalently bound hetero dyads is the electronic communication between the subunits leading to additional unfavorable photochemistry. We addressed this challenge by applying the *meta*-rule, for the first time, to a *meta*-hybrid dyad. Thereby, we aim at achieving orthogonal switching in this system. Another crucial and often limiting aspect for the application of photoswitches is their UV

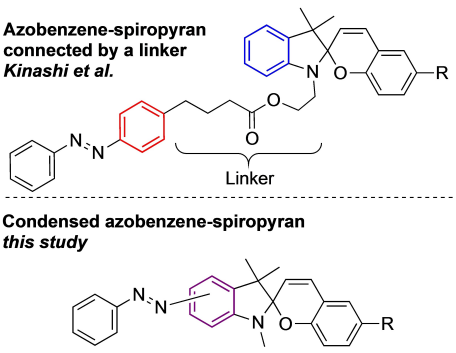

Figure 1. Comparison of the azobenzene – spiropyran dyad used by Kinashi et al.[16] and the condensed system in this study.

[*] T. Saßmannshausen,[+] Prof. Dr. J. Wachtveitl
Institute of Physical and Theoretical Chemistry, Goethe University
Max-von-Laue-Straße 7, 60438 Frankfurt am Main (Germany)
E-mail: wveitl@theochem.uni-frankfurt.de

Dr. A. Kunz,[+] Prof. Dr. H. A. Wegner
Institute of Organic Chemistry, Justus Liebig University Giessen
Heinrich-Buff-Ring 17, 35382 Giessen (Germany)
and
Center of Material Research (LaMa/ZfM), Justus Liebig University
Heinrich-Buff-Ring 16, 35392 Giessen (Germany)
E-mail: Hermann.A.Wegner@org.chemie.uni-giessen.de

N. Oberhof,[+] F. Schneider, Prof. Dr. A. Dreuw
Interdisciplinary Center for Scientific Computing, Heidelberg University
Im Neuenheimer Feld 205, 69120 Heidelberg (Germany)
E-mail: andreas.dreuw@iwr.uni-heidelberg.de

C. Slavov
Department of Chemistry, University of South Florida
4202 E: Fowler Avenue, Tampa, FL 33620 (USA)

[+] These authors contributed equally to this work.

absorption leading to photodegradation and photodamage. Hence, we exploit the red-shifting effect of *para*-connectivity still obtaining an orthogonally photoswitchable system consisting of AB and SP. Herein (*E*)-AB can be independently switched to (*Z*)-AB and SP to its merocyanine (MC) form.

Results and Discussion

Synthesis

To access the desired AB-SP derivatives **10**, **11**, **16** & **17**, two different synthetic routes (Route 1 & Route 2, Scheme 1) depending on the *meta* or *para* substitution pattern of the AB moiety were developed. To obtain *meta*-AB-SP (**10** & **11**), a synthesis route was selected building up the AB first and establishing the SP unit in a second step. An alternative synthesis strategy starting from SP directly did not provide the desired product. First, *meta*-iodo-aniline (**1**) was subjected to diazotation, followed by reduction to its corresponding hydrazine derivative. A Fischer indole synthesis provided iodo-indolenine **2** in 22% yield over three steps.[18] Iodo-indolenine **2** and Boc-phenyl-hydrazine **5**,which was obtained by Cu(I)-catalyzed coupling of *tert*-butyl carbazate **4** with iodobenzene (**3**), were coupled using the $Pd(OAc)_2/P(t\text{-}Bu)_3$ catalyst system to the corresponding arylhydrazidobenzene **6**. This reaction is advantageous since it can also be applied to synthesize various other *N*-(*tert*-butoxycarbonyl)phenylhydrazide derivatives, opening a convenient access to substituted AB-SPs in general.[19–21] The resulting hydrazide **6** was oxidized to indolenine-AB **7** with NBS/pyridine.[22,23] Here, prior attempts with MnO_2 as well as CuI did not result in the desired AB **7**. After methylation of indolenine-AB **7** and subsequent formation of a Fischer-base-AB intermediate, condensation with salicylaldehyde **8** leads to the formation of unsubstituted *m*eta-(*E*)-AB-SP **10**. Initial switching experiments revealed a very low half-life of the MC form of **10**. To increase the half-life, the corresponding nitro-derivatives have been synthesized. The NO_2-*m*eta-(*E*)-AB-SP **11** could be obtained from nitro-substituted salicylaldehyde **9** in an analogous way.

For the *para*-connectivity of AB and SP, unsubstituted as well as nitro-substituted SPs **13** and **14** were synthesized by condensation of Fisher base **12** with the respective salicylaldehydes **8** or **9**.[24] With **13** and **14** in hand, electrophilic aromatic substitution with diazonium salt **15** provided *para*-(*E*)-AB-SP **16** as well as its nitro-substituted analogue **17**. In both cases, purification was very challenging due to the opening of the SP moiety to the MC form, which affected the yield of the final compounds drastically.

Spectral properties of para-(E)-AB-SP

In agreement with previous findings for unsubstituted *para*-bis-AB the *para*-(*E*)-AB-SP **17** shows a strongly red-shifted absorption spectrum,[9] which is dominated by the typical ππ* absorption peak of AB red-shifted to 385 nm compared to unsubstituted AB. The red-shift is due to the electron donating effect of the indoline ring (Figure 2 A). The unsubstituted AB and SP were used as a monomeric model system. According to our theoretical calculations on **17** as well as the individual monomers, (5-indonlinyl)-AB (*para*-indole-AB) and SP, reveal the SP and the AB to be decoupled within **17**. The low-energy transitions are strictly located either on the AB or the SP part. (Figure 3, Table 1). The spiroatom separates the typical AB excited states from those of SP.

Excitation with light of 405 nm wavelength allows for exclusive conversion of the (*E*)-AB unit, which can be seen in the corresponding photostationary state PSS405 with no characteristic MC band. The presence of a pronounced

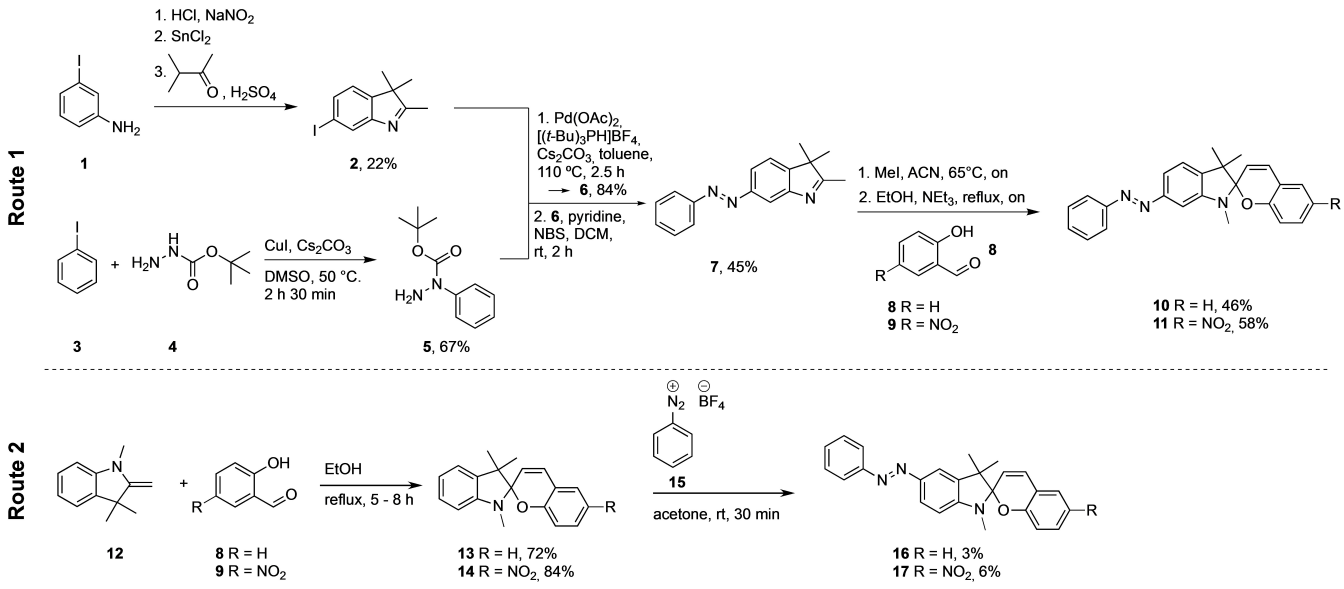

Scheme 1. Synthesis of AB-SP derivatives **10**, **11**, **16** & **17**.

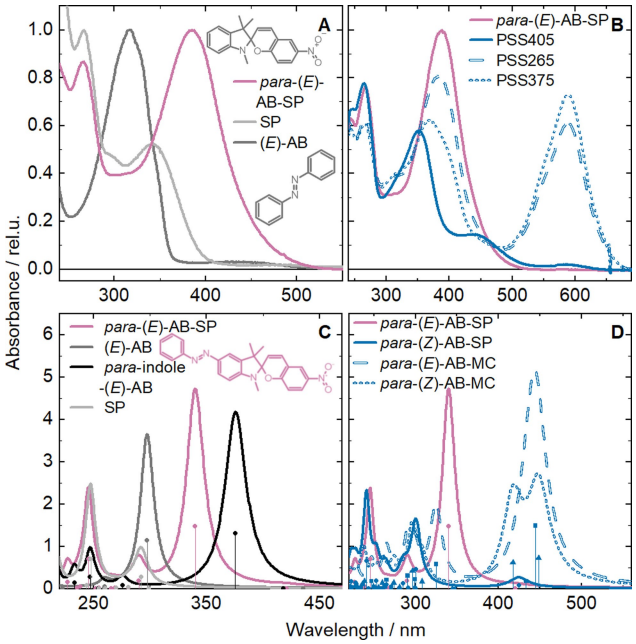

Figure 2. A & C: Normalized UV/Vis absorption spectra (A) and calculated absorption spectra (C) of the two monomers in dark (AB) and light (SP) grey, *para*-(*E*)-AB-SP in purple and *para*-indole-AB in black (only C). B: Photostationary states (PSS) at 405, 375 and 265 nm after continuous illumination at 10 °C. D: Calculated absorption spectra of all four isomers of **17**. Calculated absorption spectra were computed at CAM-B3LYP/6-311G* D3(BJ) PCM(MeCN) level of theory.

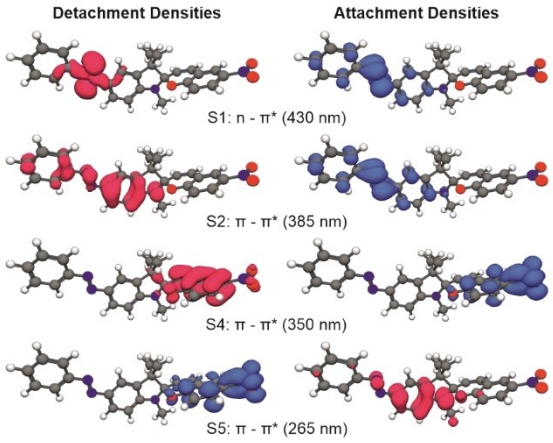

Figure 3. Detachment/Attachment (red/blue) densities of the relevant electronic transitions of *para*-(*E*)-AB-SP **17** calculated at CAM-B3LYP/6-311G* D3(BJ) PCM(MeCN) level of theory and depicted with an isovalue of 0.002. S3 omitted due to nitro group localization and zero oscillator strength.

absorption at 450 nm (nπ* state of (*Z*)-AB), however, indicates that in PSS405 predominantly the *para*–(*Z*)-AB-SP derivative of **17** is formed. (Figure 2 B). The detachment/attachment densities of the excited state corresponding to the transition at 405 nm is in fact mostly due to the ππ* absorption of the (*E*)-AB moiety (Figure 3). The thermal half-life of the (*Z*)-isomer is relatively short with 6 min at

Table 1: Localization, character of transition, and central wavelengths of the lowest peaks in the absorption spectra of *para*-(*E*)-AB-SP and, for comparison, also of the *para*-(*Z*)-AB-SP and *para*-(*E*)-AB-MC isomers accessed via irradiation in the corresponding photostationary states.

Band	Transition	λ/nm
Para-(E)-AB–SP		
E-AB (S_1)	nπ*	430
E-AB (S_2)	ππ*	385
SP (S_4, chromene)	ππ*	350
SP (S_5, chromene/indoline)	ππ*	265
para-(Z)-AB–SP		
Z-AB	nπ*	435
Z-AB	ππ*	350
para-(E)-AB–MC		
MC	ππ*	585
MC	ππ*	405

10 °C. Thus, the exact composition of PSS405 cannot be determined by NMR.

The *para*-(*E*)-AB-SP to *para*-(*Z*)-AB-MC conversion shows an excitation wavelength dependence. After initial $E \rightarrow Z$ isomerization, wavelengths close to 350 and 435 nm promote the $Z \rightarrow E$ back reaction. Continuous irradiation with light of 375 nm leads to the photostationary state PSS375, which compared to the initial spectrum shows additional absorption around 450 nm and the typical MC absorption above 550 nm, indicating the switching of both moieties and formation of *para*-(*Z*)-AB-MC (Fig.s. 2 B/D).

Individual switching of the SP moiety to MC by excitation at 350 nm is not possible due to the spectral overlap and the higher extinction coefficient of the AB moiety. However, **17** exhibits a distinct UV band around 265 nm (Fig.s. 2 B/D), which can be assigned to an excited state localized at the SP part (Figure 3 S5). Indeed, the corresponding photostationary state PSS265 shows a dominant MC contribution, while the intensity of the typical ππ* band of the (*E*)-AB part decreases only slightly, indicating that *para*-(*E*)-AB-MC is predominantly formed by individually switching the SP moiety to MC leaving (*E*)-AB mostly untouched. However, *para*-(*E*)-AB-MC has a high thermal relaxation rate with a half-life of only 100 s at 10 °C in acetonitrile returning back to *para*-(*E*)-AB-SP.

Ultrafast dynamics of para-(E)-AB-SP

According to the analysis of the different photostationary states, transient absorption (TA) experiments on *para*-(*E*)-AB-SP **17** with 400 nm excitation wavelength address the ultrafast dynamics initiated at the (*E*)-AB unit, i.e. the individual switching of (*E*)-AB to (*Z*)-AB within **17** (Figure 4 A). The ground state bleach (GSB) signal is observed between 360 and 400 nm and is present over the complete observation time. Up to about 4 ps, two excited state absorption (ESA) bands are visible between 420–660 nm and below 350 nm, respectively. The long-lived positive signal

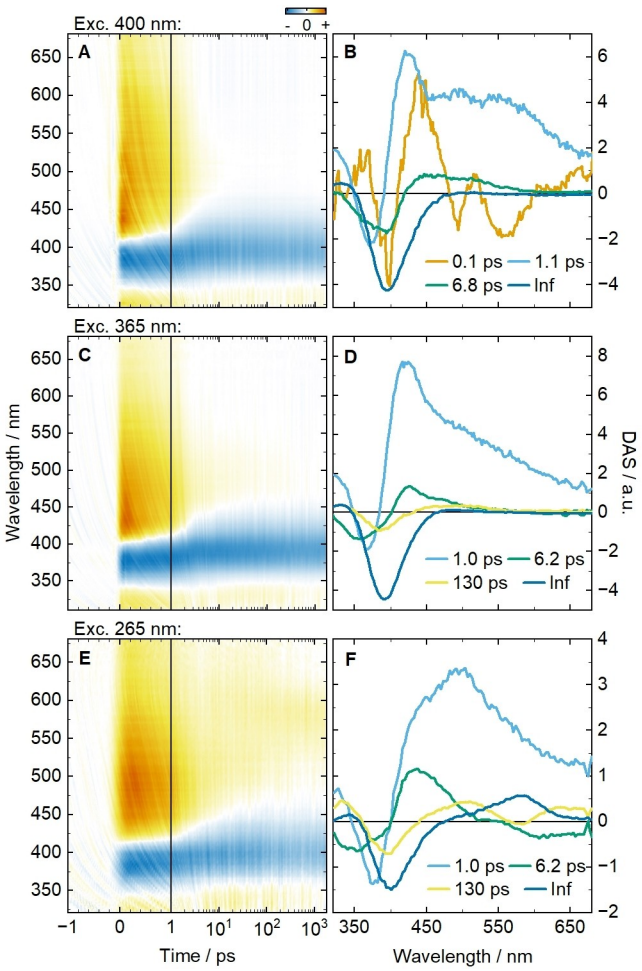

Figure 4. Transient absorption spectra of *para*-(*E*)-AB-SP after excitation with 400 nm (A), 365 nm (C) and 265 nm (E) light and the corresponding DAS (B, D and F). For A, C and E positive signals indicate product absorption (PA) or excited state absorption (ESA). The negative signals refer to ground state bleach (GSB) or stimulated emission (SE). In B, D and F, the positive components describe a rising negative or a decaying positive signal. The negative component depicts a decaying negative or a rising positive signal.

below 350 nm is associated with the formation of *para*-(*Z*)-AB-SP.

To determine the kinetics and to identify transient species, the transient absorption data can be accurately fitted with four monoexponential functions (Figure 4 B). While the shortest lifetime of 0.1 ps is related to the $S_2 \rightarrow S_1$ relaxation located at the (*E*)-AB moiety, the second time constant of 1.1 ps corresponds to the return to the electronic ground state S_0, since the GSB and the two ESA signals decay. The cooling of the hot ground state is described by the third lifetime of 6.8 ps. The infinite lifetime on the timescale of the experiment corresponds to the (*Z*)-AB photoproduct, since the decay associated spectrum (DAS) reflects its absorption spectrum as well as the remaining GSB (385 nm). This behavior is complementary to the ultrafast dynamics of the AB monomer (see SI, Figure 3).

TA measurements on *para*-(*E*)-AB-SP **17** with excitation pulses of 365 nm display very similar dynamics. The GSB and the two ESA signals show analogous temporal behavior. However, a small positive signal around 450 nm rises during the first few picoseconds and can be associated with *para*-(*E*)-AB-MC triplet formation.[25] The DAS of the first two (1.0 ps and 6.2 ps) and the infinite lifetime show common spectral features to the 400 nm excitation. But, a satisfactory description of the data requires an additional, longer lifetime component of 130 ps to account for the decay of the positive signal around 400–500 nm, which can be assigned to the decay of the triplet state of MC (Figure 4 D).

Additionally, we excited *para*-(*E*)-AB-SP **17** with 340 nm light, i.e., on the high-energy side of the ππ* band located at the (*E*)-AB moiety. The transient spectra show enhanced MC dynamics on the 100 ps timescale as well as the 150 ps as seen in the corresponding DAS (SI, Fig.s. 3 & 4). Most likely, one main absorption band located on the SP unit is present at around 340 nm, which is very similar to the band in isolated SP. This indicates, that the electronic properties of SP are not as strongly altered in **17** compared to those of the significantly red-shifted AB unit. This is confirmed by theoretical calculations which determine this SP transition to be located on the chromene part of SP unit and therefore to be decoupled from the AB unit by the spiro atom (Figure 3 S4).

TA experiments with 265 nm excitation reveal, that the SP→MC reaction is further enhanced (Figure 4 E), but still shows AB dynamics due to energy transfer from the SP to the AB moiety. The initial broad ESA signal also stretches from 430–680 nm, but the intensity distribution is shifted to higher wavelengths. The GSB and ESA signals are similar to the preceding experiments. After 10 ps, the unique MC signal around 550 nm becomes visible and persists beyond the experimentally accessible time window (>2 ns). To confirm common SP→MC dynamics upon 365 nm and 265 nm excitation, both corresponding datasets were combined and analyzed together. The analysis results in an accurate fit for both datasets with pronounced SP→MC dynamics in the 265 nm experiment and a conserved AB dynamic. The detailed inspection of the corresponding lifetimes and DAS reveals also new spectral features (Figure 4 F). The maximum of the DAS of the 1.0 ps lifetime component is shifted by 50 nm compared to the previous experiments with longer excitation wavelengths and has a similar position as the second DAS of the SP monomer (SI, Figure 2). For **17**, this DAS reflects a mixture of typical AB and MC ESA decay and the corresponding GSB recovery. The hot ground state of the AB moiety, and the formation of the triplet state[25] of *para*-(*Z*)-AB-MC are reflected in the 6.2 ps component. It additionally shows the formation of an- MC species above 560 nm. The third lifetime of 130 ps and the latter process describes the biexponential formation of the MC product. The infinity spectrum reflects an MC isomer absorbing around 580 nm and indicates (*E*)-AB→(*Z*)-AB photoisomerization through the remaining large GSB at 375 nm. (Figure 4 F).

Spectral properties of meta-(E)-AB-SP

Similar to the unsubstituted *meta*-bis-AB, which consists of two electronically uncoupled AB units, the spectrum of *meta*-(*E*)-AB-SP **11** comes very close to the sum of the spectra of the individual AB and SP monomers (Figure 5 A).[9] The ππ* band of the (*E*)-AB moiety can be clearly identified at 325 nm, while its nπ* band is hidden under a tail around 400 nm (Table 2). The latter can be identified in the calculated absorption spectrum as an additional transition, characterized as charge transfer (CT) state (Figure 5 C, Figure 6 S2). It corresponds to an electronic excitation from the indoline π-system into the π*-orbital localized at the azo unit (Figure 6 S2). A contribution to the absorption spectrum of *meta*-(*E*)-AB-SP originating from the SP unit appears as a small bathochromic shoulder of the main band around 350–375 nm. The weaker intensity of the peaks originating from the SP moiety is due to the threefold lower extinction coefficient of SP compared to (*E*)-AB. Overall, our quantum chemical calculations on *meta*-(*E*)-AB-SP **11** and the individual constituents, (6-indolinyl)-AB (*meta*-indole-AB) and SP, qualitatively agree with the experimental findings even though vibrational effects and explicit solvent interations are not included. They confirm the spectral overlap between the ππ* state of (6-indolinyl)-AB and the lowest excited state of SP located at the chromene unit (Figure 5 C). Most importantly, the calculations show the conservation of spectral features of the photoswitches upon individual switching of the other unit (Figure 5 D). The detachment/attachment densities highlight the electronic separation of both moieties. The first three transitions here are located on the AB unit while the next transition is localized on the chromene of SP, being decoupled by the spiroatom (Figure 6). These theoretical findings predict orthogonal switching behavior of the AB and SP moieties within **11** and suggest the *meta*-rule, initially derived for *bis*-AB, to be transferable to hybrid AB-SP systems. Accordingly, irradiation of *meta-(E)*-AB-SP with 420 nm light excites the CT and nπ* states located at the (*E*)-AB moiety. Analysis of the resulting photostationary state (PSS420; Figure 5 B, solid line) shows exclusive composition of *meta*-(*E*)-AB-SP and *meta*-(*Z*)-AB-SP, and no character-

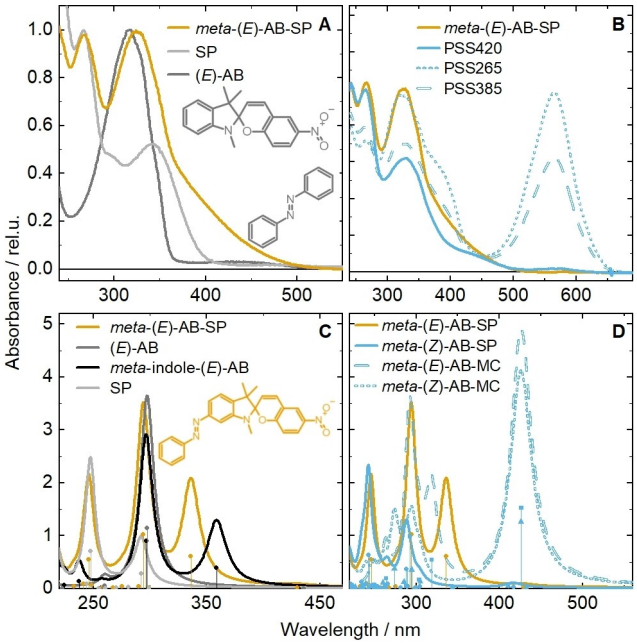

Figure 5. Normalized UV/Vis absorption spectra (A) and calculated spectra (C) respectively of the two monomers in dark (AB) and light grey (SP), *meta*-(*E*)-AB-SP in orange and *meta*-indole-AB in black (only C). PSS at different excitation wavelengths (solid, dashed and dotted lines) at 20 °C (B) and the calculated spectra of all relevant isomers of **11** (D). Calculated absorption spectra were computed at CAM-B3LYP/6-311G* D3(BJ) PCM(MeCN) level of theory.

Table 2: Band positions, orbital characters, and central wavelengths of *meta*-(*E*)-AB-SP and, for comparison, also of the *meta*-(*Z*)-AB-SP and *meta*-(*E*)-AB-MC isomers accessed via irradiation in the corresponding photostationary states.

Band	Transition	λ/nm
meta-(*E*)-AB-SP		
(*E*)-AB (S_1)	nπ*	430
(*E*)-AB (S_2)	CT	400
(*E*)-AB (S_3)	ππ*	325
SP (S_5, chromene)	ππ*	340
SP (S_6, chromene/indoline)	ππ*	265
meta-(*Z*)-AB-SP		
(*Z*)-AB	nπ*	435
(*Z*)-AB	ππ*	350
meta-(*E*)-AB-MC		
MC	ππ*	565
MC	ππ*	395

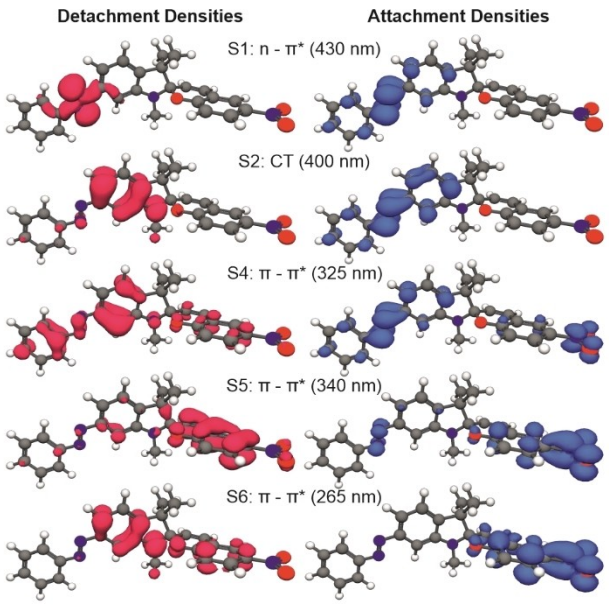

Figure 6. Detachment/attachment (red/blue) densities of the important transitions of *meta*-(*E*)-AB-SP **11** calculated at CAM-B3LYP/6-311G* D3(BJ) PCM(MeCN) level of theory and depicted with an isovalue of 0.002. S3 omitted due to nitro group localization and zero oscillator strength.

istic MC band at 560 nm being present. *Meta*–(*Z*)-AB-SP has a thermal relaxation half-life of several hours, which allowed us to perform an ^{1}H NMR experiment on PSS420 resulting in 56 % *meta*-(*Z*)-AB-SP and 44 % *meta*-(*E*)-AB-SP (SI, Fig.s. 6–8). The photoconversion ratio of these isomers is limited by their strongly overlapping nπ* bands at the AB unit above 400 nm leading to their nearly 1 : 1 mixture in PSS420.

The highest level of (*E*)→(*Z*) conversion accompanied of SP→MC conversion was achieved upon continuous illumination with 385 nm light in PSS385 (Figure 5 B, dashed line). In contrast the largest MC concentration with simultaneous (*E*)→(*Z*) conversion was obtained by irradiation with 365 nm light (SI, Figure 9). This is due to significant spectral overlap at 365 nm between the ππ* states located at the (*Z*)- and (*E*)-AB parts (Table 2) preventing significant accumulation of the (*Z*)-isomer.

Similar to **17**, our calculations indicate that the 265 nm band belongs to an electronic transition of **11**, which is located at its SP moiety (Figure 6 S6). Thus, irradiation at 265 nm (Figure 5 B, dotted line) avoids direct excitation of the (*E*)-AB part and subsequent (*E*)→(*Z*) photoconversion. This leads to predominant formation of *meta*-(*E*)-AB-MC without observable change in the bands associated with the (*E*)-AB unit in the photostationary state PSS265. However, MC has a moderate thermal relaxation rate with a half-life of $\tau_{1/2} \approx 100$ s at 20 °C, which limits the accumulation of *meta*-(*E*)-AB-MC.

Ultrafast dynamics of meta-(E)-AB-SP

Transient absorption spectroscopy on *meta*-(*E*)-AB-SP **11** after 430 nm excitation yields a spectrum (Figure 7 A) with a broad (370–600 nm) ESA signal, which lasts until 3.9 ps resembling (*E*)-AB dynamics (see SI Figure 3). Due to its low extinction coefficient, the GSB signal at 430 nm originating from the nπ* state at the (*E*)-AB part of **11** is not resolved (SI, Material and Methods). For analysis, the data was accurately fitted with only two exponential decay functions (Figure 7 B) of which the second, dominant lifetime (3.9 ps) describes the decay of the ESA related to the AB moiety. Compared to the parent AB compound[9] (see SI Figure 3), the AB integrated in this hybrid dimer shows a prolonged excited state lifetime. Since the GSB signal originating from the ππ* excitation of the AB part lies outside the detected spectral range, the infinite spectrum is flat (see SI, Material and Methods).

Excitation with 340 nm light (Figure 7 C), yields a similar ESA signal, also lasting up to 4 ps. Overall the ESA contribution is broadened to 650 nm, and at later timescales an additional positive absorption signal around 550 nm is visible consistent with SP→MC photoconversion. Below 350 nm, the GSB is apparent and partially compensated by the overlapping ESA signal. After 10 ps, when the ESA has decayed, the GSB signature spectrally broadens to match the corresponding ground state absorption spectrum of *meta*-(*E*)-AB-SP. This TA experiment thus reveals excited state dynamics of both photochromic units initiated by 340 nm excitation (Figure 7 D).

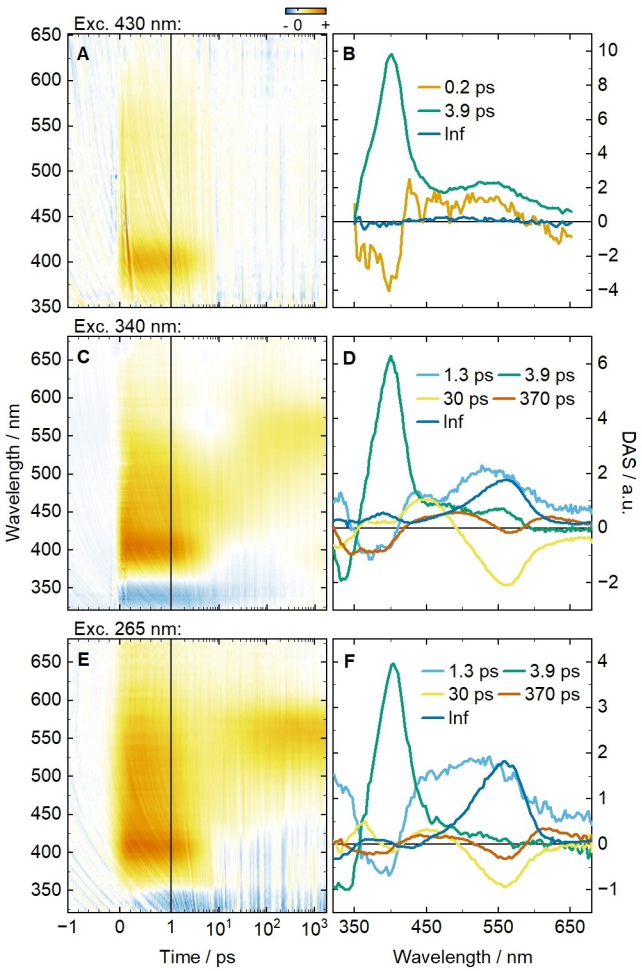

Figure 7. Transient absorption spectra of *meta*-(*E*)-AB-SP on the left and the corresponding DAS on the right side. The color code is as in Figure 3. For A, C and E positive signals indicate product absorption (PA) or excited state absorption (ESA). The negative signals refer to ground state bleach (GSB) or stimulated emission (SE). In B, D and F, the positive components describe a rising negative or a decaying positive signal. The negative component depicts a decaying negative or a rising positive signal.

To disentangle the excited-state dynamics, we fitted the two datasets (after 340 nm and after 430 nm excitation) together. The 3.9 ps lifetime, obtained in the analysis of the 430 nm experiments, which accounts for *meta*-(*E*)-AB-SP→*meta*-(*Z*)-AB-SP switching, was fixed in the joint analysis. Thus, the remaining lifetime components and their DAS should exclusively describe the underlying SP→MC dynamics.

The 1.3 ps lifetime of **11** shows an ESA signal above 420 nm which is related to the MC triplet decay. Similar to the SP monomer, the corresponding DAS shows a positive contribution below 350 nm, which describes the decay of a second ESA contribution of the MC band (SI, Figure 2). This component is only weakly visible in the experimental data due to the significant overlap of this ESA with the GSB of AB.

The negative TA signal between 360 and 420 nm (Figure 7 C) after 10 ps is also found in the monomer (SI, Figure 2) and accounts for the recovery of the GSB of *meta*-(*E*)-AB-SP. The fourth lifetime component (30 ps) is spectrally similar to the 30 ps component in the monomer (SI, Figure 2) and describes GSB recovery of *meta*-(E)-AB-SP at 350 nm, while the positive feature around 450 nm describes the decay of the *meta*-(*E*)-AB-MC triplet state.[25] Following the analysis of Holm et al.,[25] the fourth (30 ps) and fifth (370 ps) components describe the biexponential formation of a similar MC triplet isomer absorbing at 550 nm. The infinite lifetime eventually depicts the absorption of the SP→MC switching at 550 nm[25] and the (*E*)→(*Z*) conversion at 325 nm. The analysis of the 265 nm experiment (Figure 7 E) is analogous. However, as expected from the PSS-analysis, the features of the SP→MC dynamics is significantly more pronounced. Notably, (*E*)-AB dynamics are still detectable in the transient absorption data, indicating that a completely independent excitation of the SP moiety between 260–280 nm is not feasible. This effect is strongly pronounced in the TA data due to low extinction coefficient of SP relative to AB. The behavior can also be derived from the deattachment/attachment densities (Figure 6 S6) since they are distributed over the whole SP moiety. For the PSS265 (Figure 5), a (*Z*)→(*E*) back reaction takes place, which prevents accumulation of the (*Z*)-isomer. This indicates the largely independent excitation of both subunits and thus, yielding an uncoupled system where the AB and SP moieties undergo independent dynamics after excitation.

Conclusion

The understanding of multifunctional molecular systems like the presented hybrid photochromic compounds **11** and **17** are an important step towards the building of versatile, controllable multifunctional nanostructures and materials. These two novel hybrids presented here consist of an AB and a SP covalently linked in a *meta*- or *para*-configuration. The presence of multiple photoswitches within one molecule yields complex interactions and possibly intertwined photodynamics. Photochromic homodyads are relatively well studied but typically lack selective addressability of the individual parts. This possibility is generally offered by hybrid dimers.

The absorption spectrum of *para*-(*E*)-AB-SP is red shifted by 60 nm. Our experiments and the theoretical calculations reveal the important transitions for SP are located on the chromene moiety. Thus, the spiro-connection electronically decouples the latter transition from the AB unit and hence this SP transition is not strongly influenced by *para* substitution. While the different isomers *para*-(*E*)-AB-SP, *para*-(*Z*)-AB-SP and *para*-(*Z*)-AB-MC are easily accessible by irradiation with light of appropriate wavelength, *para*-(*E*)-AB-MC is not exclusively accessible due to concomitant (*E*)→(*Z*) switching of the AB unit.

As expected, *meta*-connectivity further promotes the electronic decoupling of the two photoswitchable subunits, which can be addressed individually in steady state experiments. An additional charge-transfer transition from the indoline moiety to the π* orbital of the AB enables individual excitation of the (*E*)-AB unit in **11** and *meta*-(*E*)-AB-SP→*meta*-(*Z*)-AB-SP switching. However, *meta*-(*E*)-AB-SP→*meta*-(*E*)-AB-MC switching is again accompanied by some (*E*)→(*Z*) switching due to energy transfer from the SP to the AB moiety in **11**. While *meta*-AB-SP **11** is a promising orthogonally switchable bifunctional molecular system, the red-shift due to *para*-substitution in *para*-AB-SP **17** allows for improved addressability still yielding a decoupled system.

In summary, the detailed photophysical analysis of AB-SP hybrid photochromic dyads provides a deep understanding of the underlying switching and quenching mechanisms and gives design guidelines central to the development of complex photoswitchable molecular structures.

Supporting Information

The authors have cited additional references within the Supporting Information.[26–34]

Acknowledgements

The authors acknowledge financial support by the Deutsche Forschungsgemeinschaft (DFG) within the Research Unit FOR 5499 "Molecular Solar Energy Management - Chemistry of MOST Systems" (project 496207555). T.S. acknowledges financial support by the Stiftung Polytechnische Gesellschaft Frankfurt (SPTG). J.W. and C.S. acknowledge the DFG (WA 1850/4-3) for funding. Open Access funding enabled and organized by Projekt DEAL.

Conflict of Interest

The authors declare no conflict of interest.

Data Availability Statement

The data that support the findings of this study are available in the supplementary material of this article.

Keywords: Connectivity—Meta Rule · Hybrid Photoswitch · Multifunctional Materials · Quantum Chemistry · Ultrafast Spectroscopy

[1] Z. L. Pianowski, *Chem. Eur. J.* **2019**, *25*, 5128–5144.
[2] A. Goulet-Hanssens, F. Eisenreich, S. Hecht, *Adv. Mater.* **2020**, *32*, 1905966.
[3] L. Sun, Y. A. Diaz-Fernandez, T. A. Gschneidtner, F. Westerlund, S. Lara-Avila, K. Moth-Poulsen, *Chem. Soc. Rev.* **2014**, *43*, 7378–7411.
[4] C. L. Sun, C. Wang, R. Boulatov, *ChemPhotoChem* **2019**, *3*, 268–283.
[5] A. Lennartson, A. Roffey, K. Moth-Poulsen, *Tetrahedron Lett.* **2015**, *56*, 1457–1465.

[6] M. Irie, *Chem. Rev.* **2000**, *100*, 1685–1716.
[7] F. Cisnetti, R. Ballardini, A. Credi, M. T. Gandolfi, S. Masiero, F. Negri, S. Pieraccini, G. P. Spada, *Chem. Eur. J.* **2004**, *10*, 2011–2021.
[8] J. Robertus, S. F. Reker, T. C. Pijper, A. Deuzeman, W. R. Browne, B. L. Feringa, *Phys. Chem. Chem. Phys.* **2012**, *14*, 4374–4382.
[9] C. Slavov, C. Yang, L. Schweighauser, C. Boumrifak, A. Dreuw, H. A. Wegner, J. Wachtveitl, *Phys. Chem. Chem. Phys.* **2016**, *18*, 14795–14804.
[10] C. Boumrifak, C. Yang, S. Bellotto, H. A. Wegner, J. Wachtveitl, A. Dreuw, C. Slavov, *ChemPhotoChem* **2019**, *3*, 411–417.
[11] A. Kunz, H. A. Wegner, *ChemSystemsChem* **2021**, *3*, e2000035.
[12] A. U. Petersen, J. Kirschner Solberg Hansen, E. Sperling Andreasen, S. Peder Christensen, A. Tolstrup, A. Bo Skov, A. Vlasceanu, M. Cacciarini, M. Brøndsted Nielsen, *Chem. Eur. J.* **2020**, *26*, 13419–13428.
[13] M. M. Lerch, M. J. Hansen, W. A. Velema, W. Szymanski, B. L. Feringa, *Nat. Commun.* **2016**, *7*, 12054.
[14] K. Kinashi, Y. Ueda, *Mol. Cryst. Liq. Cryst.* **2006**, *445*, 223/[513]–230/[520].
[15] K. Kinashi, K. Furuta, Y. Harada, Y. Ueda, *Chem. Lett.* **2006**, *35*, 298–299.
[16] K. Kinashi, Y. Ono, Y. Naitoh, A. Otomo, Y. Ueda, *J. Photochem. Photobiol.* **2011**, *217*, 35–39.
[17] G. R. Wilson, K. C. Park, G. C. Thaggard, C. R. Martin, A. R. Hill, J. Haimerl, J. Lim, B. K. P. Maldeni Kankanamalage, B. J. Yarbrough, K. L. Forrester, R. A. Fischer, P. J. Pellechia, M. D. Smith, S. Garashchuk, N. B. Shustova, *Angew. Chem. Int. Ed.* **2023**, *62*, e202308715.
[18] L. Wu, Y. Dai, X. Jiang, C. Petchprayoon, J. E. Lee, T. Jiang, Y. Yan, G. Marriott, *PLoS One* **2013**, *8*, e64738.
[19] L. Jiang, X. Lu, H. Zhang, Y. Jiang, D. Ma, *J. Org. Chem.* **2009**, *74*, 4542–4546.
[20] Z. Wang, R. T. Skerlj, G. J. Bridger, *Tetrahedron Lett.* **1999**, *40*, 3543–3546.
[21] M. Wolter, A. Klapars, S. L. Buchwald, *Org. Lett.* **2001**, *3*, 3803–3805.
[22] C. Wang, X. Wang, Y. Wang, *IJC-B* **1999**, *38B*, 964–965.
[23] Y.-K. Lim, K.-S. Lee, C.-G. Cho, *Org. Lett.* **2003**, *5*, 979–982.
[24] C. J. Roxburgh, P. G. Sammes, A. Abdullah, *Dyes Pigm.* **2011**, *90*, 146–162.
[25] A. K. Holm, O. F. Mohammed, M. Rini, E. Mukhtar, E. T. J. Nibbering, H. Fidder, *J. Phys. Chem. A* **2005**, *109*, 8962–8968.
[26] A. H. Heindl, H. A. Wegner, *Beilstein J. Org. Chem.* **2020**, *16*, 22–31.
[27] E. I. Balmond, B. K. Tautges, A. L. Faulkner, V. W. Or, B. M. Hodur, J. T. Shaw, A. Y. Louie, *J. Org. Chem.* **2016**, *81*, 8744–8758.
[28] Y. Shiraishi, M. Itoh, T. Hirai, *Phys. Chem. Chem. Phys.* **2010**, *12*, 13737–13745.
[29] Y. Shao, Z. Gan, E. Epifanovsky, A. T. B. Gilbert, M. Wormit, J. Kussmann, A. W. Lange, A. Behn, J. Deng, X. Feng, D. Ghosh, M. Goldey, P. R. Horn, L. D. Jacobson, I. Kaliman, R. Z. Khaliullin, T. Kuś, A. Landau, J. Liu, E. I. Proynov, Y. M. Rhee, R. M. Richard, M. A. Rohrdanz, R. P. Steele, E. J. Sundstrom, H. L. Woodcock, P. M. Zimmerman, D. Zuev, B. Albrecht, E. Alguire, B. Austin, G. J. O. Beran, Y. A. Bernard, E. Berquist, K. Brandhorst, K. B. Bravaya, S. T. Brown, D. Casanova, C.-M. Chang, Y. Chen, S. H. Chien, K. D. Closser, D. L. Crittenden, M. Diedenhofen, R. A. DiStasio, H. Do, A. D. Dutoi, R. G. Edgar, S. Fatehi, L. Fusti-Molnar, A. Ghysels, A. Golubeva-Zadorozhnaya, J. Gomes, M. W. D. Hanson-Heine, P. H. P. Harbach, A. W. Hauser, E. G. Hohenstein, Z. C. Holden, T.-C. Jagau, H. Ji, B. Kaduk, K. Khistyaev, J. Kim, J. Kim, R. A. King, P. Klunzinger, D. Kosenkov, T. Kowalczyk, C. M. Krauter, K. U. Lao, A. D. Laurent, K. V. Lawler, S. V. Levchenko, C. Y. Lin, F. Liu, E. Livshits, R. C. Lochan, A. Luenser, P. Manohar, S. F. Manzer, S.-P. Mao, N. Mardirossian, A. V. Marenich, S. A. Maurer, N. J. Mayhall, E. Neuscamman, C. M. Oana, R. Olivares-Amaya, D. P. O'Neill, J. A. Parkhill, T. M. Perrine, R. Peverati, A. Prociuk, D. R. Rehn, E. Rosta, N. J. Russ, S. M. Sharada, S. Sharma, D. W. Small, A. Sodt, T. Stein, D. Stück, Y.-C. Su, A. J. W. Thom, T. Tsuchimochi, V. Vanovschi, L. Vogt, O. Vydrov, T. Wang, M. A. Watson, J. Wenzel, A. White, C. F. Williams, J. Yang, S. Yeganeh, S. R. Yost, Z.-Q. You, I. Y. Zhang, X. Zhang, Y. Zhao, B. R. Brooks, G. K. L. Chan, D. M. Chipman, C. J. Cramer, W. A. Goddard, M. S. Gordon, W. J. Hehre, A. Klamt, H. F. Schaefer, M. W. Schmidt, C. D. Sherrill, D. G. Truhlar, A. Warshel, X. Xu, A. Aspuru-Guzik, R. Baer, A. T. Bell, N. A. Besley, J.-D. Chai, A. Dreuw, B. D. Dunietz, T. R. Furlani, S. R. Gwaltney, C.-P. Hsu, Y. Jung, J. Kong, D. S. Lambrecht, W. Liang, C. Ochsenfeld, V. A. Rassolov, L. V. Slipchenko, J. E. Subotnik, T. Van Voorhis, J. M. Herbert, A. I. Krylov, P. M. W. Gill, M. Head-Gordon, *Mol. Phys.* **2015**, *113*, 184–215.
[30] T. Yanai, D. P. Tew, N. C. Handy, *Chem. Phys. Lett.* **2004**, *393*, 51–57.
[31] R. Krishnan, J. S. Binkley, R. Seeger, J. A. Pople, *J. Chem. Phys.* **2008**, *72*, 650–654.
[32] S. Grimme, J. Antony, S. Ehrlich, H. Krieg, *J. Chem. Phys.* **2010**, *132*, 154104.
[33] S. Hirata, M. Head-Gordon, *Chem. Phys. Lett.* **1999**, *314*, 291–299.
[34] F. Plasser, A. I. Krylov, A. Dreuw, *WIREs Comput. Mol. Sci.* **2022**, *12*, e1595.

Manuscript received: September 25, 2023
Accepted manuscript online: December 7, 2023
Version of record online: December 20, 2023